

# Force control of a non-backdrivable robot without a force sensor

Zihan Chen and Peter Kazanzides

**Abstract**— Cooperatively controlled robots are used in many kinds of applications, including surgical robot applications where the surgeon can guide the robot end effector to a desired position. Often, a 6 degree-of-freedom (DOF) force/torque sensor is installed. However, in some cases, the sensor is only used to impose safety thresholds and to support the robot guidance task. In cases where high guidance accuracy is not required, it can be difficult to justify the added cost of a 6 DOF force sensor. One lower-cost solution is to incorporate a joystick or similar input device, but this requires additional hardware and removes the surgeon's hands from direct interaction with the robot end-effector. This paper presents a method for achieving cooperative force control without a force sensor. The method utilizes motor current feedback and uses a calibrated current value for force estimation. The novelty of this method is that it can be applied to non-backdrivable robots. It is implemented on a 2-DOF XY stage and experiments are conducted to demonstrate accuracy and performance on this non-backdrivable robot.

## I. INTRODUCTION

For human-machine systems, impedance control and admittance control are widely used to enable operator in-the-loop collaborative systems [3]. Impedance controlled robots are often lightly damped and backdrivable [7], whereas admittance controlled robots are, in general, highly geared and either non-backdrivable or difficult to backdrive. Thus, most of them use a force/torque sensor to enable guidance via admittance control, which converts the measured force (or, more generally, force error) into a desired Cartesian velocity. The interest of this paper is admittance type robots that are used in cooperative manipulation robot systems. To achieve admittance control, the most straight-forward solution is to install a 6-DOF force-torque sensor at the robot end effector, and develop the desired Cartesian space velocity based on force feedback. This solution can provide the high accuracy and reliability that are necessary for some applications, such as retinal microsurgery [10]. In other cases, however, we do not require high precision guidance of robot and the force sensor is only used for crude guidance. One example is given by a robot system for small animal research, where the force sensor was only needed to allow the user to guide the robot to fiducial markers during an initial registration [5].

Several solutions have been proposed to provide force guidance capability without requiring a wrist force/torque sensor. One approach is to install torque sensors at each joint, as done in the DLR lightweight robot [1]. If, however, the robot does not have joint torque sensors, it is also possible to estimate the joint torque from the measured motor current

Z. Chen and P. Kazanzides are with the Laboratory for Computational Sensing and Robotics, Department of Computer Science, Johns Hopkins University, Baltimore, MD 21218, USA. Peter Kazanzides can be reached at pkaz@jhu.edu.

feedback [4], assuming that the control electronics provides this feedback. The use of filtered dynamic equations has been proposed to improve the estimate of force from noisy joint torque measurements [12], which is especially a concern when motor current feedback is used. Yet another alternative is to use the position error to estimate the end-effector torque [8]. The disadvantage of this solution is that it requires detuning of the control system (i.e., to create larger position errors) and it cannot be used for non-backdrivable robots.

This paper presents an admittance-like controller for a non-backdrivable system, which allows the user to guide the robot without a force sensor. This controller is a data-based method that enables joint torque estimation in not-moving and moving cases and is implemented on a 2-axis XY stage (NEAT-6060).

## II. MOTIVATION

The motivation for this work derived from our earlier study that investigated the use of measured motor current to estimate the force applied on the rods that actuated a snake-like mechanism [4]. That system used a small DC motor and lead screw for push/pull actuation. The experiments demonstrated that the motor current feedback enabled estimation of the motor load with a resolution of less than 1 N. This level of accuracy was obtained as long as the controller was actively trying to move the motor, even at low speeds up to the onset of motor stall. As future work, we noted that “this suggests that it would be possible to obtain force feedback from motor currents in a non-backdrivable system with an appropriate control law” [4].

Clearly, it is impossible to use motor current to measure applied force in a stationary non-backdrivable system because the applied force is not transmitted to the motor. Thus, it is necessary to “cheat” a little; specifically, to apply a low amplitude periodic dither signal to the motor. This dither signal should also be relatively low frequency to avoid any unpleasant buzzing noise and subsequent mechanical wear. In general (e.g., if there is no gravity loading), one would expect the measured motor current to be symmetric about the origin, with positive current when the motor is moving in one direction and negative current when it is moving in the other direction. Intuitively, if an external force is applied during this time, it should assist motion in one direction (thereby lowering the motor current) and impede motion in the opposite direction (thereby increasing the motor current). This should cause the measured current to be asymmetric with respect to the origin and its average value should roughly indicate the direction and magnitude of the applied force. Once the axis is in motion, it should also be possible

to continue to estimate the applied force by comparing the measured current to the expected current. In this case, the expected current could be based on previously recorded data (e.g. moving the axis through its range of travel, without an applied force) or on a mathematical model.

Unfortunately, this intuitive approach does not work in practice. One counter-intuitive finding is that applying force in the direction of motion does not necessarily decrease the motor current. In some cases, the motor current increases even though the external force should be “helping” the motor, for example see Fig. 8. To explain this phenomenon, and motivate a better approach, it is necessary to first study the model of a lead screw.

### III. PHYSICAL MODEL

Lead screws are widely used to convert rotary motion to linear motion (see Fig. 1). Their mechanics are similar to the inclined plane shown in Fig. 3(a). To lift a weight  $W$ , the applied horizontal force  $F$  must be:

$$F \geq \left( \frac{\mu + \tan \lambda}{1 - \mu \tan \lambda} \right) W, \quad (1)$$

where  $\mu$  is the coefficient of friction and  $\lambda$  is the lead angle. When a force is pushing down vertically on the weight, if  $\mu > \tan \lambda$ , the weight will not move no matter how large the force is. This also explains the non-backdrivability of the lead screw drive. Fig. 2 shows the interaction between a left-handed lead screw and nut threads. Left-handed means the nut moves left when the lead screw is rotated clockwise [11]. By convention, the normal force  $N$  is positive when the nut threads and the leading lead screw threads are in contact.

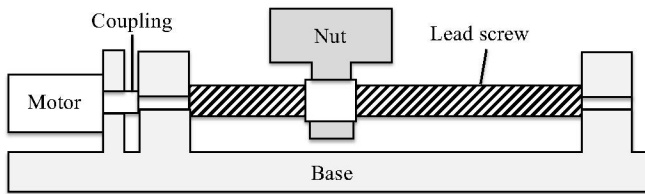


Fig. 1. Illustration of motor driving a lead screw

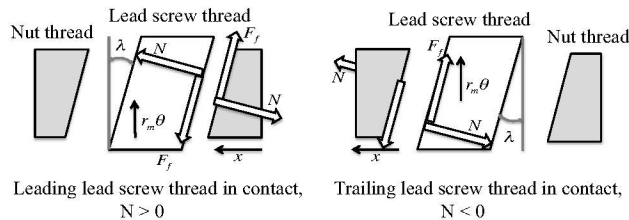


Fig. 2. Normal force sign convention. The nut (gray) is moving left. The left image shows the definition of normal force direction when the nut’s left surface is in contact with lead screw’s right surface. The right one shows the case with trailing lead screw thread.

A pair of lead screw and nut threads is shown in Fig. 3(b).  $m$  is the mass of the moving nut and  $I$  is the lead screw inertia.  $P$  is the force applied on the axial direction

and  $T$  is the applied torque. By Newton’s second law, we can write the following equations:

$$m\ddot{x} = P - N \cos \lambda - F_f \sin \lambda \quad (2)$$

$$I\ddot{\theta} = T + r(N \sin \lambda - F_f \cos \lambda), \quad (3)$$

where  $r$  is the lead screw pitch circle radius,  $\lambda$  is lead angle, and  $\theta$  is the screw rotation. We note that a more complete model would include other friction terms (e.g., for the translating nut and lead screw supports) as well as rotational and linear damping coefficients of the lead screw drive, but these can be neglected in the following analysis.

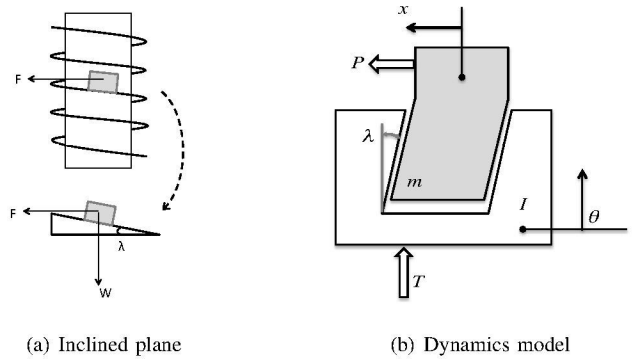


Fig. 3. Lead screw models; nut is gray and lead screw is white.  $P$  is external force on nut and  $T$  is torque on lead screw.

Linear motion of the nut,  $x$ , is related to  $\theta$  by  $x = r \tan \lambda \theta$ . The friction force  $F_f$  is equal to  $\mu_s N$ , where  $\mu_s = \mu \operatorname{sgn}(\dot{\theta}N)$ . Substituting these into (2) and (3) yields:

$$mr \tan \lambda \ddot{\theta} = P - N \cos \lambda (1 + \mu_s \tan \lambda) \quad (4)$$

$$I\ddot{\theta} = T - Nr \cos \lambda (\mu_s - \tan \lambda). \quad (5)$$

Eliminating  $\ddot{\theta}$  and solving for  $N$  yields:

$$N = \frac{PI - Tmr \tan \lambda}{I \cos \lambda (1 + \mu_s \tan \lambda) - mr^2 \sin \lambda (\mu_s - \tan \lambda)} \quad (6)$$

In general, this equation requires an iterative solution for  $N$  because the  $\mu_s$  terms on the right depend on the sign of  $N$ . But, all quantities in (6) are positive constants, except for  $P$ ,  $T$ , and  $\mu_s$ . By rearranging terms, noting that  $I < mr^2$  for the nut, and making the physically realistic assumption that  $\tan \lambda < 1$ , it can be shown that the denominator is always positive. Thus,  $\operatorname{sgn}(N)$  is determined by the sign of the numerator. If there is no external force ( $P = 0$ ), then  $\operatorname{sgn}(N) = -\operatorname{sgn}(T)$ . If the external force is acting against the motion,  $\operatorname{sgn}(P) = -\operatorname{sgn}(T)$  and the sign of the numerator does not change. If, however, the force is acting in the direction of motion, it is possible for the numerator to change sign. This will occur when  $P > Trm \tan \lambda / I$ .

The above analysis illustrates the problem with the initial approach. Assume that the robot is moving at constant velocity in the positive direction,  $\ddot{\theta} = 0$  and  $\theta > 0$ , driven by a positive motor output torque  $T$ . In this case, equation 5 simplifies to:

$$T = r \cos \lambda N (\mu_s - \tan \lambda) \quad (7)$$

If the external force is pushing against the nut ( $P < 0$ ), the normal force  $N$  will be negative and  $\mu_s = -\mu$ . The required motor torque  $T$  can be expressed as:

$$T = r \cos \lambda |N| (\mu + \tan \lambda). \quad (8)$$

If the external force is pushing with the nut ( $P > 0$ ) and  $PI - Trm \tan \lambda > 0$ ,  $N$  becomes positive and the required motor torque  $T$  can be written as

$$T = r \cos \lambda |N| (\mu - \tan \lambda). \quad (9)$$

The non-backdrivability of the lead screw system ensures that  $\mu - \tan \lambda > 0$ , thus in both situations (pushing against and with the nut)  $T$  will be a positive value. This also implies that for a given positive motor output torque  $T$ , there are two solutions for  $P$ , one positive and one negative. This analysis is consistent with experimental data, which shows that positive and negative forces can both increase motor current. The same effect can be shown when the motor is moving in the negative direction.

The above behavior (multiple solutions for a given motor torque) makes a purely model-based approach difficult to implement. Friction in the lead screw (mentioned above, but omitted in the equations) is another issue. An accurate friction model is essential for accurate external force estimation. However, while most models assume that the coefficient of friction is constant (e.g., Coulomb or kinetic friction) or velocity-dependent (e.g., viscous friction), friction may also depend on position. This is demonstrated in Fig. 4, which shows a motor current plot when the robot is moving at  $\dot{x} = +3$  mm/s and  $\dot{x} = +10$  mm/s when  $P = 0$ .

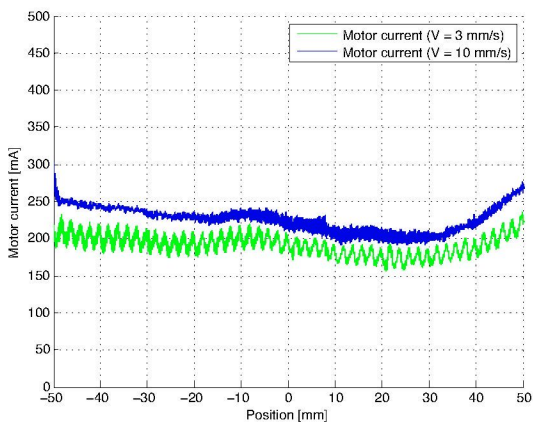


Fig. 4. Friction map at  $V = 3$  mm/s and  $V = 10$  mm/s

Finally, a model-based approach requires measurement of the motor torque,  $T$ , and the angular acceleration,  $\ddot{\theta}$ . It is well known that the torque reading will be extremely noisy when based on motor current measurement [9]. Similarly, most robots are only equipped with position encoders. Although it is possible to get good velocity estimates from encoder feedback [2], it is necessary to numerically differentiate to obtain acceleration, which introduces significant noise. Recent work by Damme et al. [12] attempts to address this problem by applying a stable first-order filter to both sides

of the dynamic equation to avoid direct calculation of the acceleration term.

The above issues led us to instead consider a data-based approach, which is described in the following section.

#### IV. TECHNICAL APPROACH

In general, the robot controller can be divided into two control modes: *robot not moving* and *robot moving*, which are detailed in Sec. IV-A and IV-B, respectively. The control block diagram Fig. 5 shows how these two control modes are connected and gives an overview of the control system (note that the *Moving Mode* also includes negative speeds, which are not shown in the figure). Starting from the not-moving state, the controller waits until the external force direction has been sensed, then shifts into moving control mode, where the motor current feedback helps to choose an appropriate motion based on the applied external force. If the measured external force is close to 0, the controller returns to the not-moving control mode.

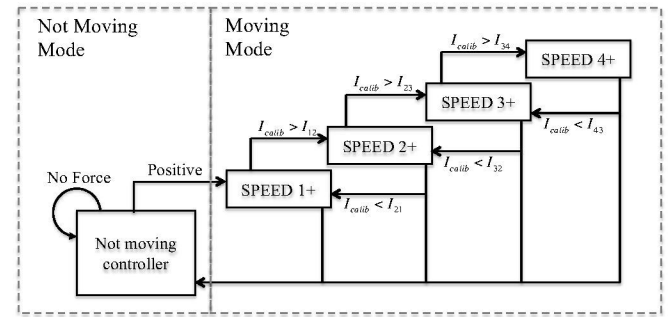


Fig. 5. Controller state diagram (negative speed states not shown)

##### A. Robot Not Moving

For a cooperatively-controlled robot, the start point of the control is to determine the operator's intention of where to move the robot. This problem can be divided into two sub-questions: (i) Is the user pushing the robot? (ii) If the user is trying to move, in which direction? Even without a force sensor, it is a simple task for an impedance type robot because it can be derived by measuring the robot position offset. However, a non-backdrivable system, by definition, cannot be moved by an external force. To solve this dilemma, we apply a sawtooth wave to the motor and measure the minimum motor current needed to make the system start moving. One operation cycle comprises the four phases shown in Fig. 6, where  $I_{cmd}$  is the commanded motor current,  $v_m$  is the measured motor velocity, and  $I_{pos}$  and  $I_{neg}$  are the smallest commanded motor currents that caused motion in the positive and negative directions, respectively. At the end of each actuating cycle, the  $I_{pos}$  and  $I_{neg}$  values are used to estimate the external force direction. On average, one complete cycle takes 100 ms.

Fig. 7(a) plots the mean and standard deviation of  $I_{pos}$  and  $I_{neg}$ , when we applied -20 N, -10 N, -5 N, 0 N, 5 N, 10 N, 20 N force to the robot Y axis. When the external force is 0 N, the actuating motor only needs to generate

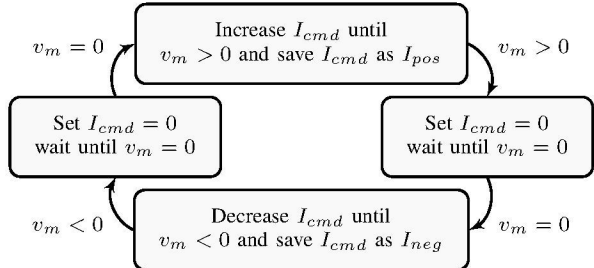
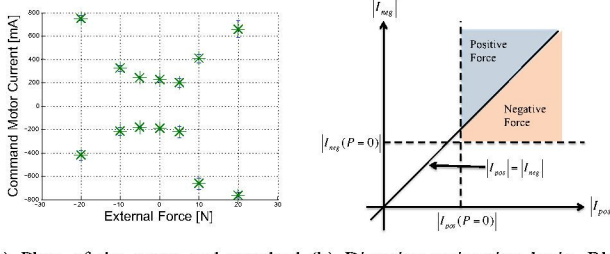


Fig. 6. Current search block diagram

torque to overcome the friction force. However, when there exists an external force, both  $I_{pos}$  and  $I_{neg}$  will increase, indicating that more torque is needed to start moving the robot for both directions. The figure also shows that given a positive external force,  $|I_{neg}|$  is larger than  $|I_{pos}|$  due to the fact that the positive external force is against the moving direction. These two observations are the answers to the two questions. Based on these, a simple direction estimation has been developed (see Fig. 7(b)).



(a) Plots of the mean and standard deviation of  $I_{pos}$  and  $I_{neg}$ , with different  $P$  values  
(b) Direction estimation logic. Blue zone indicates positive external force, where  $I_{pos}$  and  $I_{neg}$  are larger than zero force values and  $I_{neg} > I_{pos}$ . Red zone indicates a negative external force.

Fig. 7. Force estimation data and algorithm

This algorithm has been tested by running it at 10 evenly spaced positions along the robot axis and comparing its estimation result with the known force directions during a 2 minute time period. The results showed that it is robust in the sense that it works equally well along the entire axis and always gives the correct estimation. Further, the sawtooth wave actuating signal makes sure that the robot will not have noticeable movement before the force direction has been measured. For the hardware setup described in Section V-A, the absolute translational move is less than 0.1 mm after 20 seconds of operation.

### B. Robot Moving

The previous section discusses force direction sensing for a non-backdrivable system. The goal for the robot moving case is to command the robot velocity under an admittance law as:

$$\dot{x}_d = K_a f, \quad (10)$$

where  $\dot{x}_d$  is the desired robot Cartesian velocity,  $K_a$  is the admittance gain, and  $f$  is the measured external force/torque. To implement this algorithm on our non-backdrivable system, a measurement of external force is required.

**1) Force magnitude estimation:** As noted above, friction makes it difficult to accurately estimate force based on motor current. Because friction varies over the range of travel, one solution is to perform a calibration procedure to map the friction. Specifically, the motor is moved at a specified constant velocity  $\dot{\theta}_0$  with no external force ( $P = 0$ ) and the motor current feedback  $I_{m0}(\theta)$  is recorded along the entire lead screw. Because the friction is velocity-dependent, this mapping procedure must be repeated at different velocities. Then, it is possible to fit the data to the friction model to enable interpolation of the friction at any arbitrary velocity. We chose a simpler approach, which is to limit the motion of the motor to a discrete number of velocities, which happen to correspond to the velocities at which we mapped the friction. The motor current is calibrated by subtracting the motor current value from the current position map, and the calibrated value is proportional to external force.

Fig. 8 compares current before friction map calibration and after the calibration versus position; measured force is also plotted for reference. During the experiment,  $P$  changes from +15N to 0N then to -15N. The figure shows that the calibration procedure smooths current feedback and zeros it when  $P$  is 0 N. Pushing in both directions increases the calibrated motor current. The “pushing against” case has a much higher current versus force ratio. Calibrated motor current also matches well with the force reading from a force sensor, indicating the effectiveness of the calibration procedure and of the proposed estimation method.

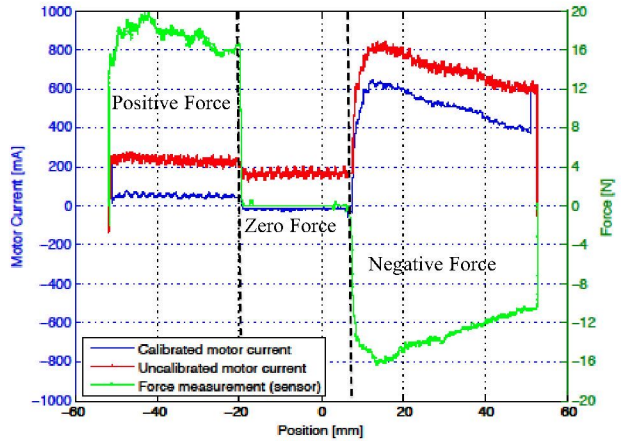


Fig. 8. Comparison between calibrated and uncalibrated motor current, data collected on one axis moving at  $V = 3$  mm/s

**2) Force Direction:** Given that external force in both directions will increase motor current feedback in same direction, it is impossible to tell force direction purely based on the current feedback value. For this reason, we assume that the applied force remains in the same direction once we are in the robot moving state. For application like cooperative control, it is a fair assumption because when a user changes pushing force direction,  $P$  value will drop to 0 N and the controller will switch to the not-moving control state, where it can once again estimate the direction of the applied force.

3) *Speed Switching*: When running at constant velocity, the motor current feedback gives an accurate and robust measurement of the force magnitude, under the assumption that the direction of the force is known. However, the constant velocity requirement is not consistent with the goal of an admittance-like controller.

Our solution is to operate the robot at a few pre-defined speed levels and to change the speed level based on calibrated current feedback. If the calibrated current is smaller (larger) than a threshold value, the controller will shift the speed down (up). Also note that the calibration current map is velocity dependent; thus, it needs to be measured for each chosen velocity level for both directions. The speed level switcher contains four speed levels for each direction. The highest level speed  $|v_4|$  is chosen so that the robot can be moved through its range of travel within 5 seconds.

## V. EXPERIMENTS

The aforementioned controller has been implemented on a 2-axis XY stage and experiments were performed to evaluate its performance.

### A. Hardware Setup

Our hardware setup consists of a NEAT-6060 high precision linear XY stage actuated by brush motors. Fig. 1 shows the lead screw drive structure for one joint. The lead screw-nut interface converts the motor rotational motion to translation and provides non-backdrivability of the robot. The motor is directly coupled with the lead screw without a gearbox and has an encoder mounted to provide position measurement. Joint velocities are computed from the encoder feedback. Finally, the system is powered by a custom linear amplifier board, with IEEE-1394a (Firewire) interface, that controls the motor current and provides motor current feedback measurement.

A centralized processing and distributed I/O control structure (see Fig. 9) [6] is used to control the system. A Linux workstation communicates with the robot via a low-latency, high-speed serial IEEE-1394a bus with direct access to the I/O data. The control loop runs at 1kHz and does all the computations.

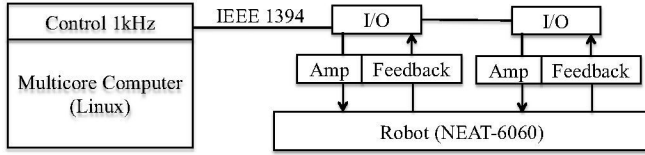


Fig. 9. Block diagram of controller setup

### B. Performance study

For the performance test, a 6 DOF ATI force/torque sensor was installed on the robot to be used as ground truth and also to compare the performance of the proposed method with the conventional force-sensor based admittance control.

During the test, the robot is controlled by the proposed method running in the positive direction. The robot velocity,

calibrated motor current and measured force are recorded. For an ideal admittance controller, the command velocity  $\dot{x}_{cmd}$  is computed based on (10) with  $K_a = 0.4$  using the measured force data. Figure 10 compares command velocities from these two controllers, which shows that the proposed controller has comparable performance with an admittance controller, except that it is less sensitive.

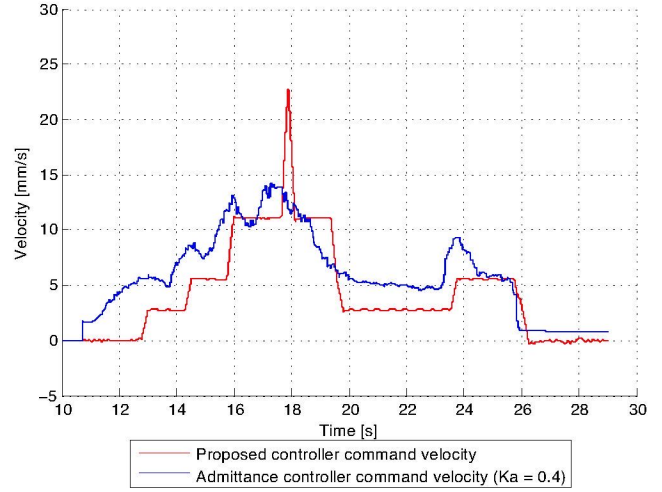


Fig. 10. Command velocities comparison between 2 controllers: (i) Admittance controller based on force sensor feedback; (ii) Proposed controller without force sensor

An estimation of force is also computed from the calibrated motor current and compared with the measured force (see Fig. 11). The estimated force shows good agreement with the measured force. One limitation is that the force estimation only works in the robot-moving control state (between 13 s to 26 s). This explains the noisy “estimated force” at the start and stop conditions.

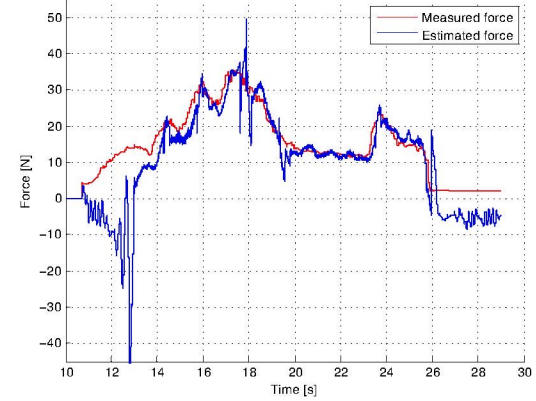


Fig. 11. Comparison of estimated force and measured force obtained during velocity test

### C. Positioning Task

A positioning task is designed to compare the performance of the proposed controller to a conventional admittance controller using a force sensor. For reference, a graphical user interface (GUI) is also implemented as an alternative to the proposed method, as neither one requires the use of a

force sensor. The GUI contains 9 buttons (see Fig. 12(b)) and operates much like a rate-controlled joystick. For example, pressing the “>” button will cause the robot to slowly move to the right, whereas pressing “>>” will cause it to move more quickly to the right. In either case, the motion will continue until the middle button (labeled “-”) is pressed.

To perform this task, a laser pointer is mounted vertically on the robot end effector. In the task, the user is required to move the robot to a series of 9 predefined positions in sequence, so that the laser pointer position is within 1.5 mm of the target position, as determined by visual observation. Each task is performed 5 times and the average times are compared. To make the task comparable, the three controllers are designed to have the same maximum velocity. For the controller with the force sensor, a basic admittance control law (10), with maximum response force of 8 N, is used.

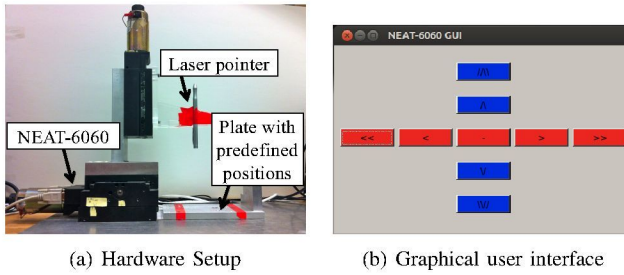


Fig. 12. Robot Positioning Test

As shown in Fig. 13, the average time with the proposed method is 100.76 seconds, with the force sensor is 48.52 seconds, and with the GUI is 72.46 seconds. Our proposed method shows comparable performance in this two-dimensional positioning task. Although it doubles the time to complete the task compared with admittance controller with a force sensor, it is more intuitive than the GUI and eliminates the need for a force sensor.

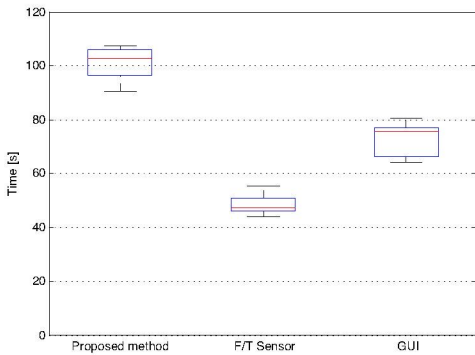


Fig. 13. Positioning task: average time cost to complete a positioning task using proposed controller, F/T sensor with admittance control and a graphical interface control

## VI. CONCLUSIONS

We presented a method to achieve admittance-like force control for a non-backdrivable robot system based on motor current feedback. Of course, this is impossible when the

non-backdrivable robot is stationary, so it is necessary to apply a small dither signal during the “not-moving” state so that the robot is actually moving a little bit. With a careful choice of dither signal, we have found the motion to be barely perceptible. The complete controller can be divided into robot not-moving and moving modes. The not-moving controller must only estimate the direction of the external force and then transition to the positive or negative moving mode. Once in a moving mode, the algorithm assumes that the direction of motion does not change, and therefore must only estimate the magnitude of the applied force. If the force magnitude increases beyond a threshold, the controller transitions to the next higher speed. Conversely, if the magnitude decreases, it transitions to the next lower speed or to the “not-moving” state. An experiment was conducted to compare performance of this controller for a simple positioning task to the more conventional controller using a force sensor (which would be a more costly solution) and to a graphical user interface for positioning the robot (which also does not require a force sensor). The presented method shows acceptable performance and appears to be suitable for coarse positioning tasks.

## ACKNOWLEDGMENT

Paul Thienphrapa provided the initial FPGA code for the robot controller hardware.

## REFERENCES

- [1] A. Albu-Schäffer, S. Haddadin, C. Ott, A. Stemmer, T. Wimböck, and G. Hirzinger. The DLR lightweight robot: design and control concepts for robots in human environments. *Industrial Robot: An International Journal*, 34(5):376–385, 2007.
- [2] P. Bhatti and B. Hannaford. Single chip velocity measurement system for incremental optical encoders. *IEEE Trans. Control Systems Technology*, 5(6):654–661, Jun 1997.
- [3] K. Hashtroodi-Zaad. Analysis of Control Architectures for Teleoperation Systems with Impedance/Admittance Master and Slave Manipulators. *The International Journal of Robotics Research*, 20(6):419–445, June 2001.
- [4] A. Kapoor, N. Simaan, and P. Kazanzides. A system for speed and torque control of DC motors with application to small snake robots. *Mechatronics and Robotics*, 2004.
- [5] P. Kazanzides, J. Chang, I. Iordachita, J. Li, C. C. Ling, and G. Fichtinger. Development of an image-guided robot for small animal research. *Computer Aided Surgery*, 12(6):357–365, Nov 2007.
- [6] P. Kazanzides and P. Thienphrapa. Centralized processing and distributed I/O for robot control. In *IEEE Int'l. Conf. on Technologies for Practical Robot Applications (TePRA)*, pages 84–88, Nov 2008.
- [7] P. Marayong. *Motion control methods for human-machine cooperative systems*. PhD thesis, Dept. of Mechanical Engineering, The Johns Hopkins University, 2008.
- [8] A. Stolt, M. Linderoth, A. Robertsson, and R. Johansson. Force controlled robotics assembly without a force sensor. In *Proc. IEEE Int'l. Conf. on Robotics and Auto. (ICRA)*, pages 1538–1543, May 2012.
- [9] J. Swevers, C. Ganseman, D. Tukel, J. de Schutter, and H. Van Brussel. Optimal robot excitation and identification. *IEEE Transactions on Robotics and Automation*, 13(5):730–740, 1997.
- [10] A. Uneri, M. A. Balicki, J. Handa, P. Gehlbach, R. H. Taylor, and I. Iordachita. New steady-hand eye robot with micro-force sensing for vitreoretinal surgery. In *BIOROB*, pages 814–819, Tokyo, Japan, Sep 2010.
- [11] O. Vahid-Araghi and F. Golnaraghi. *Friction-Induced Vibration in Lead Screw Drives*. Springer, New York, 2011.
- [12] M. Van Damme, P. Beyl, B. Vanderborght, V. Grosu, R. Van Ham, I. Vanderniepen, A. Matthys, and D. Lefeber. Estimating robot end-effector force from noisy actuator torque measurements. In *IEEE Int'l. Conf. on Robotics and Auto. (ICRA)*, pages 1108–1113, May 2011.